U.S. ARMY COMBAT CAPABILITIES DEVELOPMENT COMMAND
CHEMICAL BIOLOGICAL CENTER

ABERDEEN PROVING GROUND, MD 21010-5424

DEVCOM CBC-TR-1766

On-Demand Instrumentation: 3D Printing a Complete Ion Mobility Spectrometry Drift Tube in a Single Process

Brian C. Hauck
SCIENCE AND TECHNOLOGY CORPORATION
Belcamp, MD 21017-1427

Bradley R. Ruprecht
ENGINEERING DIRECTORATE

Patrick C. Riley
RESEARCH AND TECHNOLOGY DIRECTORATE

May 2022

Approved for public release: distribution unlimited.

Disclaimer

The findings in this report are not to be construed as an official Department of the Army position unless so designated by other authorizing documents.

REPORT DOCUMENTATION PAGE

Form Approved
OMB No. 0704-0188

Public reporting burden for this collection of information is estimated to average 1 h per response, including the time for reviewing instructions, searching existing data sources, gathering and maintaining the data needed, and completing and reviewing this collection of information. Send comments regarding this burden estimate or any other aspect of this collection of information, including suggestions for reducing this burden to Department of Defense, Washington Headquarters Services, Directorate for Information Operations and Reports (0704-0188), 1215 Jefferson Davis Highway, Suite 1204, Arlington, VA 22202-4302. Respondents should be aware that notwithstanding any other provision of law, no person shall be subject to any penalty for failing to comply with a collection of information if it does not display a currently valid OMB control number. **PLEASE DO NOT RETURN YOUR FORM TO THE ABOVE ADDRESS.**

1. REPORT DATE *(DD-MM-YYYY)*	**2. REPORT TYPE**	**3. DATES COVERED** *(From - To)*
XX-05-2022	Final	Apr 2020–May 2021

4. TITLE AND SUBTITLE
On-Demand Instrumentation: 3D Printing a Complete Ion Mobility Spectrometry Drift Tube in a Single Process

5a. CONTRACT NUMBER
2016.DLA.J3.AMC.1144.006

5b. GRANT NUMBER

5c. PROGRAM ELEMENT NUMBER
0603680S

6. AUTHOR(S)
Hauck, Brian C. (STC); Ruprecht, Bradley R.; Riley, Patrick C. (DEVCOM CBC)

5d. PROJECT NUMBER

5e. TASK NUMBER

5f. WORK UNIT NUMBER

7. PERFORMING ORGANIZATION NAME(S) AND ADDRESS(ES)
Director, DEVCOM CBC, ATTN: FCDD-CBR-ID, APG, MD 21010-5424
Science and Technology Corporation; 111 C. Bata Blvd., Belcamp, MD 21017-1427

8. PERFORMING ORGANIZATION REPORT NUMBER
DEVCOM CBC-TR-1766

9. SPONSORING / MONITORING AGENCY NAME(S) AND ADDRESS(ES)
Defense Logistics Agency; 8725 John J. Kingman Road, Fort Belvoir, VA 22060-6221

10. SPONSOR/MONITOR'S ACRONYM(S)
DLA

11. SPONSOR/MONITOR'S REPORT NUMBER(S)

12. DISTRIBUTION / AVAILABILITY STATEMENT
Approved for public release: distribution unlimited.

13. SUPPLEMENTARY NOTES

14. ABSTRACT: (Limit 200 words)
Three-dimensional (3D) printing is increasingly being used for novel applications such as constructing functional components for analytical instrumentation. 3D-printed ion mobility spectrometry (IMS) drift tubes consist of conductive and nonconductive filaments and are ideally printed in a single process. However, 3D-printed drift tubes have previously been limited to an assembly of modular subcomponents because the ion gate and aperture grid, critical subcomponents, feature freestanding wires that span the inner diameter of the drift tube. These wires cannot be easily printed above the printer bed without a support underneath. Most 3D printers are limited to either single- or dual-filament extrusion, whereas a third soluble support filament is required to print a drift tube in a single process. In this report, we present a design and single process to 3D print a complete IMS drift tube without modular assembly.

15. SUBJECT TERMS
Ion mobility spectrometry (IMS) | Three-dimensional (3D) printing | Additive manufacturing
Fused deposition modeling (FDM) | Multi-material extrusion | Rapid prototyping

16. SECURITY CLASSIFICATION OF:			**17. LIMITATION OF ABSTRACT**	**18. NUMBER OF PAGES**	**19a. NAME OF RESPONSIBLE PERSON**
a. REPORT	**b. ABSTRACT**	**c. THIS PAGE**			**19b. TELEPHONE NUMBER** *(include area code)*
U	U	U	UU	26	Renu B. Rastogi (410) 436-7545

Standard Form 298 (Rev. 8-98)
Prescribed by ANSI Std. Z39.18

Blank

PREFACE

The work described in this report was authorized by the Defense Logistics Agency (Fort Belvoir, VA), Additive Manufacturing Research and Development program, under support agreement 2016.DLA.J3.AMC.1144.006. The work was started in April 2020 and completed in May 2021.

The use of either trade or manufacturers' names in this report does not constitute an official endorsement of any commercial products. This report may not be cited for purposes of advertisement.

This report has been approved for public release.

Blank

CONTENTS

	PREFACE	iii
1.	INTRODUCTION	1
2.	METHODS	2
2.1	3D Printers	2
2.2	Filaments	2
2.3	Chemicals and Solvents	3
2.4	Printing Parameters	3
2.5	Drift Tube Design	4
2.5.1	Ion Gate	4
2.5.2	Faraday Plate and Aperture Grid	5
2.5.3	Single-Print Unibody Drift Tube	6
2.6	Data Acquisition System	7
3.	RESULTS	7
3.1	Material and Prototype Part Characterization	7
3.2	Single-Process Unibody Drift Tube	10
4.	CONCLUSIONS	12
	LITERATURE CITED	13
	ACRONYMS AND ABBREVIATIONS	15

FIGURES

1. Depiction of a typical IMS drift tube, its associated components, and resulting signal. 1
2. Designed BN ion gate at a 3 mm cross section height....5
3. (a) Top view of the designed Faraday plate/aperture grid/drift gas showerhead and (b) isometric view showing the Faraday plate below the PVA and the internal electrical leads....6
4. Dimetric and exploded cross section of the 28 cm single print unibody IMS drift tube showing (from left to right) insulating, conducting, and soluble layers 6
5. Effect of printer speed and extruder temperature on the conductivity of ESD-PETG when printed on the (a) Ender 5 and (b) ToolChanger systems 8
6. (a) Gate and (b) Faraday plate assemblies 3D-printed on the Ender 5 (left) and ToolChanger (right) systems viewed from the front and side 9
7. Drift time spectra of the $H(NH_3)^+ \bullet (H_2O)_n$ reactant ion peak at varying GPWs when using (a) the gate and Faraday plate printed on the ToolChanger system, (b) the gate printed on the Ender 5 system and the Faraday plate printed on the ToolChanger system, and (c) the gate and Faraday plate printed on the Ender 5 system 10
8. (a) Completed single-process unibody drift tube before dissolution of PVA and (b) D*t*BP spectra collected at 280 V/cm with a 200 us GPW (blue) and at 424 V/cm with a 100 μs GPW (red) 11

TABLE

1. Filament Splicing Settings in Chroma Software....3

ON-DEMAND INSTRUMENTATION: 3D PRINTING A COMPLETE ION MOBILITY SPECTROEMTRY DRIFT TUBE IN A SINGLE PROCESS

1. INTRODUCTION

Fused deposition modeling (FDM) is a three-dimensional (3D) printing method in which molten filament from a heated extruder is deposited in a predetermined pattern according to a computer-aided design (CAD) file to produce an object.[1,2] Novel applications of FDM include manufacturing parts for ion mobility spectrometry (IMS), which is an analytical technique for separating and identifying analytes such as biomolecules, explosives, and chemical warfare agents.[2–8] An IMS drift tube (Figure 1) consists of a series of electrodes separated by insulators to which a voltage gradient (V) is applied. A gaseous sample mixture is ionized and pulsed by an ion gate into the drift region. Once there, it separates based on differing ion interactions with a countercurrent neutral drift gas of known temperature (T) and pressure (P). Ions neutralize on a Faraday plate, and the drift time (t_d) across the length (L) between gate and detector is recorded. Ions are identified based on their reduced ion mobility (K_0) values, as shown in eq 1.[3]

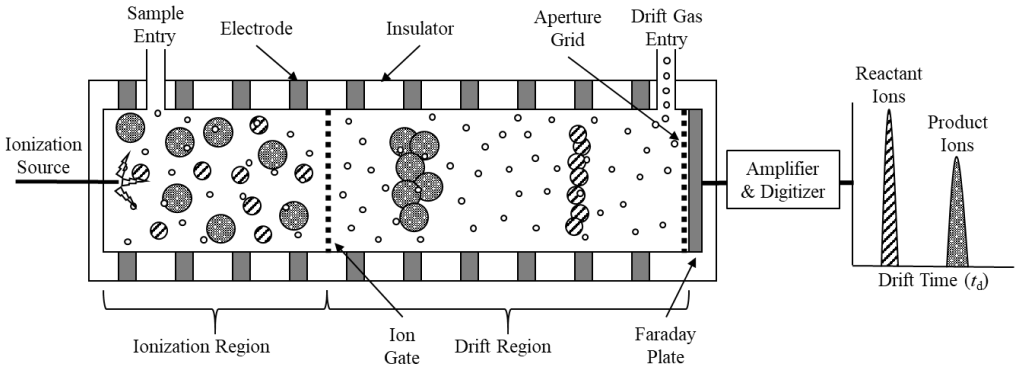

Figure 1. Depiction of a typical IMS drift tube, its associated components, and resulting signal.

$$K_0 = \frac{L^2}{V t_d}\left(\frac{273.15}{T}\right)\left(\frac{P}{760}\right) \quad (1)$$

Manufacturing drift tubes by FDM has a number of potential benefits. First, current processes may introduce error into L.[9] Second, FDM would significantly decrease the costs and production times of research grade instruments and eliminate the skilled labor required to machine metals and ceramics. Third, 3D printing is an on-demand method and could simultaneously produce multiple drift tubes at the time and point of need. When a drift tube is contaminated or broken, a new one could be 3D printed immediately.

3D printing is ideally completed in a single process to eliminate any labor associated with post processing or assembly of separate parts. Furthermore, a single process eliminates any error in the L value resulting from assembly. Unibody subcomponents, including

electrodes, ion gates, and Faraday plates, can be 3D printed using dual extrusion FDM in which the printer alternates between two nozzles, one dedicated to conductive filaments and the other to nonconductive filaments.[1] However, drift tubes printed using this technique are still modular, and the subcomponents have to be assembled by hand because the wires of the ion gate and aperture grid span the inner diameter of the final assembly. Those wires, therefore, cannot be printed above the printer bed.[9,10] Unsupported wires for these subcomponents could be extruded using bridging settings in the slicing program in which a fan rapidly cools the filament and changes are made to the flow rate, extrusion temperature, or print speed.[11–13] However, this may affect filaments where the conductivity is dependent on some or all of these settings.[9,14,15] Bridging may also be a difficult or unreliable way to create thin wires on a flat plane to preserve the *L* value and electric field homogeneity. Therefore, to 3D print a drift tube in a single process, a third soluble support filament is needed to support wires during printing. In this work, we utilized two 3D printing systems capable of combining at least three filaments to print freestanding wires for the gate and Faraday plate subcomponents. The result was the first non-modular design and process for 3D printing a complete IMS drift tube.

2. METHODS

2.1 3D Printers

Two 3D printing systems were used: a modified Ender 5 3D printer (Creality; Shenzhen, China) interfaced to a Palette 2 multi-filament splicer (Mosaic Manufacturing Ltd.; Toronto, Canada) with a 2S upgrade kit, and a ToolChanger and Motion system (E3D-Online; Oxfordshire, UK). The Palette 2 splicer was able to fuse up to four separate filaments into a single strand that was fed into the extruder of the 3D printer. Multiple materials were printed within a single layer by purging the previous filament and priming the next filament in a transition tower to the side of the print. The Bowden extruder on the Ender 5 printer was replaced with a Hemera direct drive extruder (E3D-Online), and the Palette 2 splicer was used in accessory mode. The ToolChanger system featured four independent extruders that could each be dedicated to a single filament. The system switched between filaments by docking and picking up the appropriate extruder for each stage of the print. The ToolChanger system used V6 all metal hot ends and Titan extruders (E3D-Online).

2.2 Filaments

Natural colored MAX-G polyethylene terephthalate glycol-modified (PETG) filament (3DXTECH; Grand Rapids, MI) was used to generate electrically insulating sections of the drift tube. Electrostatic dissipative (ESD)-PETG filament (3DXTECH) was used to generate the electrically conductive electrodes, gate, aperture grid, and Faraday plate. Soluble layers were generated on the Ender 5 system using soluble release (SR)-30 soluble filament (Stratasys; Rehovot, Israel) and on the ToolChanger system using polyvinyl alcohol (PVA) water-soluble filament (Raise3D; Irvine, CA). SR-30 filament had to be used with the Ender 5 printer because PVA was not compatible for splicing with the two PETG filaments in the Palette 2. All filaments were 1.75 mm in diameter.

2.3 Chemicals and Solvents

After the printing process was completed, PVA was dissolved in deionized (DI) water, and SR-30 was dissolved in a WaterWorks solution (Stratasys). 2,6 di-*tert*-butyl pyridine (D*t*BP) was obtained as a 97% pure standard from Sigma-Aldrich (St. Louis, MO) and used as a mobility calibrant.

2.4 Printing Parameters

Parts were modeled and assembled in SolidWorks 2019 CAD software (Dassault Systèmes; Vélizy-Villacoublay, France). Parts made of the same filament were exported as single stereolithography (.stl) files and imported into Simplify3D slicing software (Simplify3D; Cincinnati, OH). The appropriate profile was selected for the 3D printer that was being used. Separate processes were created for each filament and assigned to separate tools in the program. The program sliced the assembly and exported it as G-code (.gcode) files. When the Ender 5 printer and Palette 2 splicer were in use, the .gcode file was imported into Chroma 3 software (Mosaic Manufacturing; Toronto, ON) to be modified for filament transitions and create a mutation annotation format (.maf) file. The Palette 2 splicer used the .maf file to execute filament splicing and transitions in sync with the 3D printer. In Chroma, variable transitions were used with a minimum transition length of 180 mm, maximum transition length of 230 mm, and target position of 40%. The minimum density of the transition tower was 40%, with an 80% minimum bottom density and a 100% maximum density. PETG and SR-30 filaments were designated as "weak" colors, and the ESD-PETG filament was designated as a "strong" color in the Chroma program. Table 1 lists the settings used to splice together each filament combination in the Palette 2 splicer.

Table 1. Filament Splicing Settings in Chroma Software

Incoming Filament	Outgoing Filament	Heat	Compression	Cooling
SR-30	ESD-PETG	5	5	1
ESD-PETG	SR-30	6	6	
SR-30	PETG	5	5	
PETG	SR-30	6	6	
ESD-PETG	PETG	4	4	
PETG	ESD-PETG	4	4	

Assemblies were printed along the axis of ion drift in the direction of drift gas flow. Bed temperature was set to 70 ºC, and extrusion temperatures were 240, 275, 240, and 220 ºC for PETG, ESD-PETG, SR-30, and PVA, respectively. Printing speed was 2400 mm/min for all filaments on the Ender 5 system and ESD-PETG on the ToolChanger system. The ToolChanger system used a printing speed of 3600 mm/min for PETG and PVA filaments. Outline underspeeds were 50% for all filaments. Solid infill underspeeds were 80% for all filaments except for ESD-PETG, which had a solid fill underspeed of 50%. First layer underspeeds were 50%.

Both systems used 0.4 mm diameter brass nozzles, a 0.4 mm extrusion width, and a 0.2 mm layer height and coasted for 0.7 mm at the end of each extrusion. The ToolChanger system used a 100% extrusion multiplier and retracted 6.00 mm at 3600 mm/min, whereas the Ender 5 system used a 90% extrusion multiplier and retracted 10.00 mm at 1800.0 mm/min. The Ender 5 system used a 0.8 mm vertical lift for all filaments, whereas the ToolChanger system only used a lift for the ESD-PETG filament. The ToolChanger system wiped the nozzle for 5.0 mm for the PETG and ESD-PETG filaments, with retraction performed during the wipe movement. The ToolChanger system also performed retraction when crossing open layers for only the PETG and PVA filaments. The Ender 5 system did not use a wipe movement, but retractions were forced between layers. On both systems, parts made from PETG and ESD-PETG filaments were created with two outlines and three top and bottom solid layers. Soluble layers made from PVA and SR-30 filaments were created with two outlines but no solid layers to aid in dissolution. Outlines were not crossed for travel movements. All parts featured a 25% rectilinear infill with 15% outline overlap except for the SR-30, which had a 50% rectilinear infill to aid dissolution. Nano Polymer Adhesive (Vision Miner; Irvine, CA) was used as a bed adhesive. After the parts were printed and the supports were dissolved, parts were cleaned by sonicating for 1 h in Liquinox solution (Alconox, White Plains, NY) and then 1 h in DI water to prevent off-gassing. Parts were placed in an oven at 50 ºC and flushed with clean, dry air for five days.

2.5 Drift Tube Design

The ion gate and Faraday plate were initially designed as separate modular subcomponents to test their printability and functionality when inserted into a previous modular assembly featuring 3D-printed unibody drift tube sections, traditional ion gates, and a time-of-flight mass spectrometer as the detector.[9] Parts had the same general dimensions of 6 cm outside diameter (o.d.) × 5 cm inside diameter (i.d.) as these previously printed drift tube sections. A 9 mm wide × 5 mm tall section protruded from the top of the parts to allow space for the connection of electrical leads within 1.78 mm diameter × 6.5 mm deep holes. Electrical leads were attached by hand-tapping the holes for 2-56 threaded stainless steel rods. The actual colors of the PETG, ESD-PETG, and PVA filaments were clear, black, and white, respectively. However, for clarity, they are colored white, black, and yellow, respectively, in figures within this report.

2.5.1 Ion Gate

Multiple types of ion gates exist. All typically consist of one or more plane of wires orthogonal to the ion path and spanning the i.d. of the drift tube. For example, a Bradbury–Nielson (BN) design has two interleaved and electrically isolated sets of wires on the same plane, whereas a Tyndall–Powell (TP) design has the two sets of wires on adjacent planes.[16] A BN design was chosen for this experiment because successful 3D printing of its compact and complex geometry would indicate that simpler designs, such as the TP or reverse-field types, would also be possible. Figure 2 shows the BN design at a 3 mm cross section height of the 6 mm thick ring of PETG. ESD-PETG wires were designed so that the centers of rectangular wires were at a 3 mm height within the assembly. ESD-PETG gate wires were 0.6 mm wide and

0.4 mm thick (two layer heights). Wires were spaced on 2 mm centers when printed on the Ender 5 system and 2.5 mm centers when printed on the ToolChanger system. A 49 mm diameter × 2.8 mm thick disk of PVA in the center supported the ESD-PETG wires. Gate leads of 58 mm o.d. × 55 mm i.d. were printed within the insulator, and gate wires were printed in an alternating fashion connecting to a lead on one side of the gate and terminating at a radius of 26.5 mm on the other side.

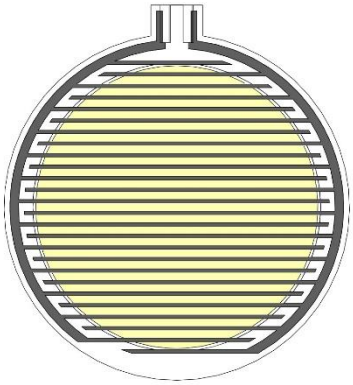

Figure 2. Designed BN ion gate at a 3 mm cross section height.

2.5.2 Faraday Plate and Aperture Grid

The Faraday plate (Figure 3) also included a drift gas entry system and an aperture grid within its assembly. The aperture grid wires had the same dimensions as the BN gate, but all wires connected to a single electrical lead at the top of the part rather than being two interleaved sets. The center plane of the wires was spaced 1 mm above the Faraday plate. Wires had the same dimensions as those in the ion gate but were 0.8 mm thick (four layer heights) to increase flexural strength. A 0.6 mm thick layer of PVA directly on top of the 0.6 mm thick Faraday plate supported the wires, and the section of PETG featuring drift gas entry holes in a showerhead formation was also printed to meet the wires and reduce their unsupported area. Leads to the aperture grid and Faraday plate led to the top of the parts and were placed on either side of a 3.4 mm diameter hole for the insertion of 1/8 in. drift gas tubing. A 2-56 threaded stainless steel rod was connected to a Bayonet Neill-Concelman (BNC) cable and screwed into the Faraday plate lead for signal transmission.

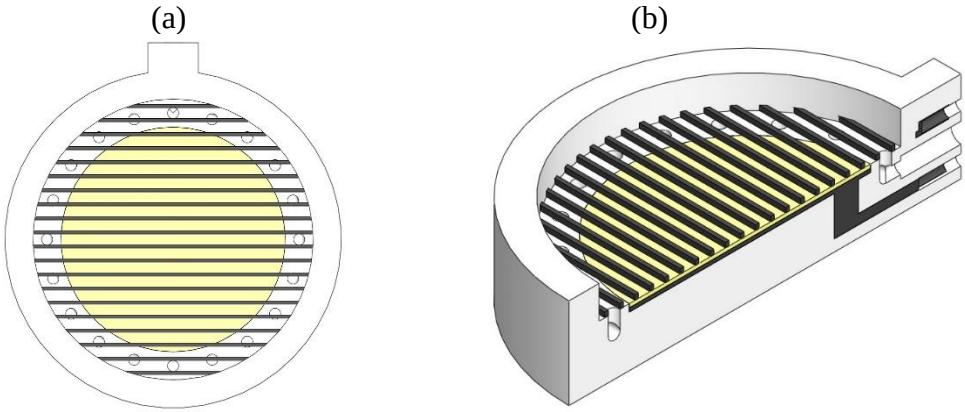

Figure 3. (a) Top view of the designed Faraday plate/aperture grid/drift gas showerhead and (b) isometric view showing the Faraday plate below the PVA and the internal electrical leads.

2.5.3 Single-Print Unibody Drift Tube

The single-print unibody IMS drift tube (Figure 4) incorporated design elements of both the individually 3D-printed ion gate and Faraday plate. The insulating shell had the same i.d. and o.d. and was 28 cm long along the axis of ion drift. Bands of ESD-PETG formed by two outlines created twenty-one 8 mm wide electrodes spaced on 10 mm centers. The drift length from the center plane of the gate wires to the surface of the Faraday plate was 14.1 cm. The first ring featured a series of wires (with the same dimensions as those in the aperture grid) across the i.d. to act as a counter electrode to a corona ionization source. The corona ionization source interfaced to the front end of the drift tube in a similar manner to a previous design.[9] To preserve filament and reduce print time, soluble layers featured lofted internal cuts before 25% infill was printed across the i.d. to support the wires of the gate and counter electrode. A hole in the reaction region allowed for the insertion of silica capillary (150 µm i.d., 360 µm o.d.; Polymicro Technologies; Phoenix, AZ) through which D*t*BP was injected from a wash bottle.

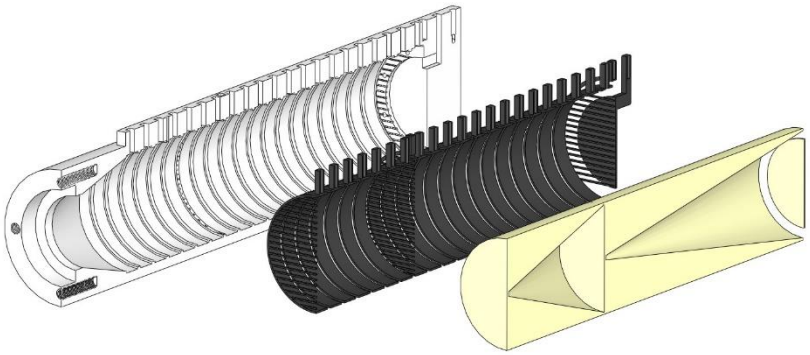

Figure 4. Dimetric and exploded cross section of the 28 cm single print unibody IMS drift tube showing (from left to right) insulating, conducting, and soluble layers.

2.6 Data Acquisition System

Parts were inserted into a previously used thermal case that heated the drift gas to 30.0 ± 0.2 ºC as measured between the two ion gates. The signal from the Faraday plate was amplified by a Model 427 current amplifier (Keithley Instruments; Cleveland, OH). The data acquisition system was controlled and spectra were recorded using a USB-6216 BNC and a previously written LabVIEW program (National Instruments; Austin, TX). Spectra consisted of 100 iterations of 20 averages. The drift tube was operated at a nominal temperature of 25 ºC as set by a CN7823 DIN temperature controller (Omega; Stamford, CT). A supply of house air (1 L/min, ~10 ppm_v H_2O) was used as the drift gas, and a permeation tube (KIN-TEK Analytical, Inc.; La Marque, TX) was used to dope the drift gas with 20 ppm_v of ammonia to reduce clustering and create a $H(NH_3)^+ \bullet (H_2O)_n$ reactant ion peak.

3. RESULTS

3.1 Material and Prototype Part Characterization

The extrusion temperature selected for the ESD-PETG filament was informed by Figure 5 in which a series of 5 mm thick electrode rings were printed as a function of both extruder temperature (between 230 and 275 ºC) and printing speed (between 30 and 60 mm/s). Rings were connected to an LS020 power supply (Exelis; West Springfield, MA) supplying 3,000.51 ± 0.08 V. Opposite the high voltage connection, a 10 GΩ high precision HVP-250 voltage divider (Computer Power Supplies; Tigard, OR) and 8846A digital multimeter (Fluke; Everett, WA) were connected to measure the conductivity and any drop in voltage across the ring. Conductivity increased at higher extrusion temperatures or lower printing speeds. The ToolChanger system exhibited a greater loss in conductivity than the Ender 5 system at lower extrusion temperatures and higher printing speeds. Differences in conductivity may have been a result of differences in the stability of the temperature set point. During extrusion, the temperatures of the hot ends on the Ender 5 and ToolChanger systems varied by ±5 and ±0.2 ºC, respectively. Differences in residence time or pressure exerted on the filament in the hot end due to using either the direct drive or Bowden setups may have also contributed to differences in conductivity. An extrusion temperature of 275 ºC and print speed of 40 mm/s was determined to be an acceptable balance of extruder temperature, filament conductivity, and print speed. In addition, the ESD-PETG filament exhibited a negligible difference in conductivity regardless of print speed at 275 ºC. Therefore, the conductivity of a part would not vary across its surface area as a result of the underspeed used to print the first layer, solid infill, or outlines. A similar ESD-PETG characterization should be done for any other 3D printing system to be used to create conductive materials.

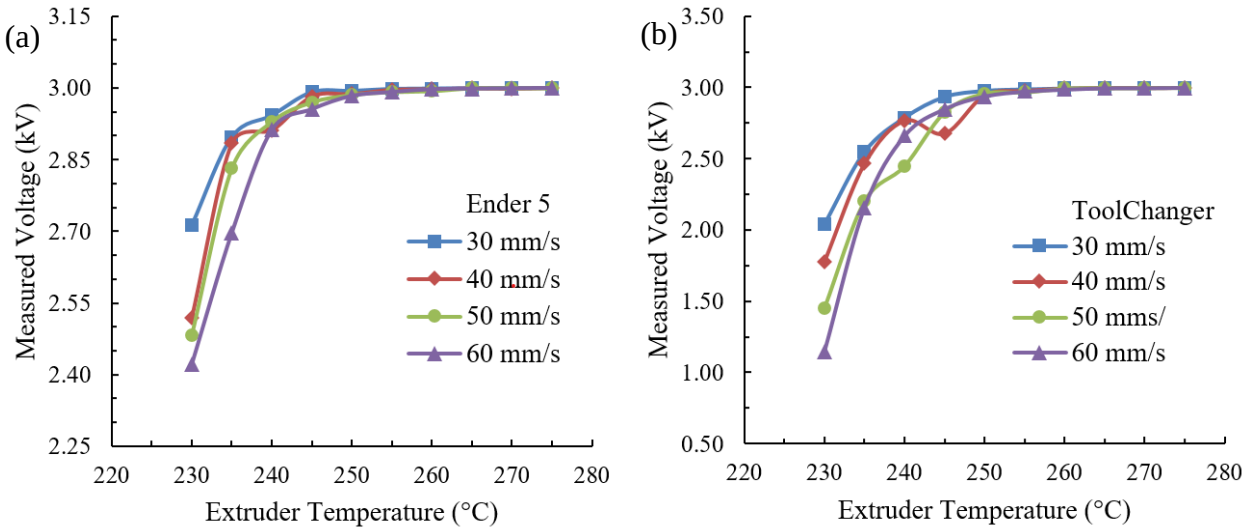

Figure 5. Effect of printer speed and extruder temperature on the conductivity of ESD-PETG when printed on the (a) Ender 5 and (b) ToolChanger systems. Error bars are contained within markers.

The Ender 5 system printed the ion gate and Faraday plate in 2 h 27 min and 6 h 3 min, respectively, whereas the ToolChanger system printed the same parts in 1 h and 2 h 18 m, respectively. Parts printed on the Ender 5 system had filament bleed within single layers because the system was unable to sufficiently purge the black ESD-PETG before printing the clear PETG. Figure 6 shows front and side views of the ion gate and Faraday plate assemblies printed on both systems. The filament bleed in the parts printed on the Ender 5 system is evident in the large bands of gray along the sides of the parts. The parts printed on the ToolChanger system did not have any filament bleed. The small vertical black lines visible in the parts printed on the ToolChanger system were the internal leads for the gate and aperture grid wires observable behind the clear outer shell of PETG.

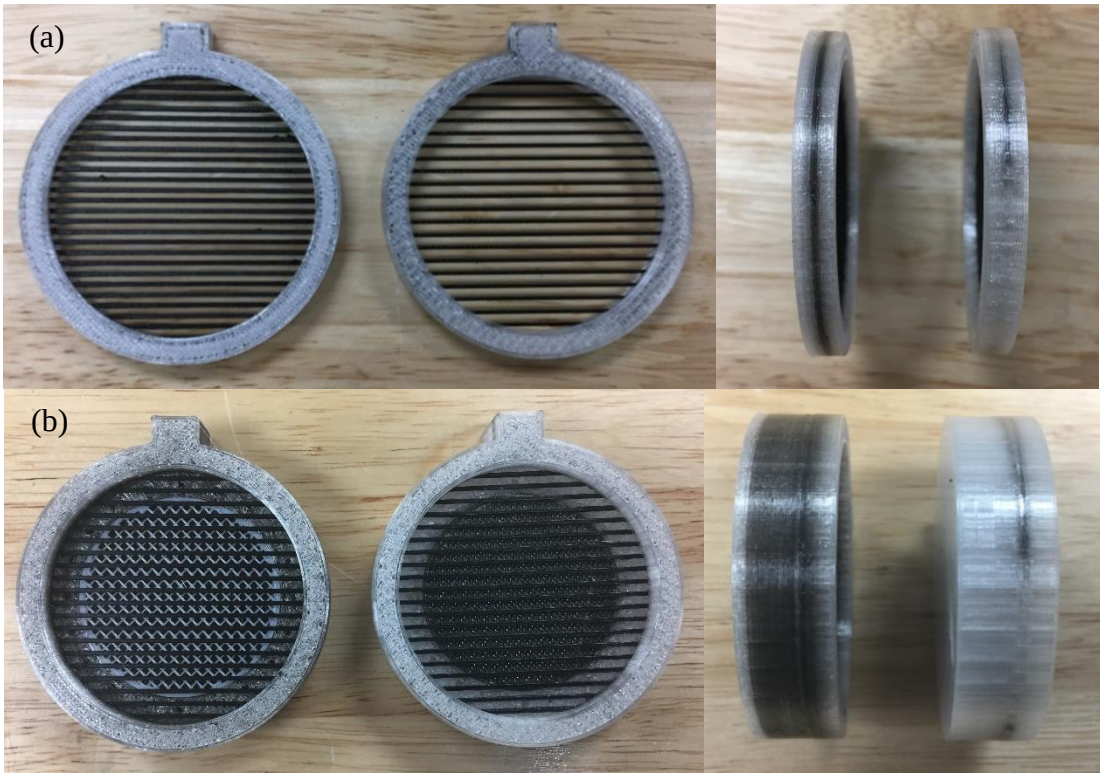

Figure 6. (a) Gate and (b) Faraday plate assemblies 3D printed on the Ender 5 (left) and ToolChanger (right) systems viewed from the front and side. Support filament is shown in the Faraday plate assemblies.

All parts functioned as intended with differences arising mainly from the different spacing of the gate wires. The gate printed on the Ender 5 system featured wires spaced on 2 mm centers, whereas the gate from the ToolChanger system had 2.5 mm centers. Wire spacing affects ion transmission into the drift region. Wires comparable in size to the gap between them hinder ion transmission, whereas wires with larger gaps between them require higher voltages to operate and block ions when the gate is in a closed state.[17] Figure 7 shows background reactant ion spectra collected from the various combinations of gates and Faraday plates printed on each system with the gate pulse width (GPW) varied between 50 and 500 μs. The calculated resolving power (R_p), a measure of peak sharpness, is shown in parentheses in the legend.[18] All spectra peak heights were normalized to the relative peak height of the highest peak in Figure 7a. The gate printed on the ToolChanger system (Figure 7a) required a gate closure voltage of ±46 V. It had higher ion transmission because of the 2.5 mm spacing of wires but lower R_p, with a maximum of 10 at a 300 μs GPW. When the gate printed on the Ender 5 system was used with the same Faraday plate printed on the ToolChanger system (Figure 7b), the required gate closure voltage was ± 21 V, and R_p increased to 23 at a GPW of 200 μs. Ion transmission decreased because of the 2.0 mm wire spacing. When the Faraday plate printed on the Ender 5 system was used with the gate printed using the same system (Figure 7c), ion transmission and R_p were maintained, but the signal to noise ratio decreased. It is possible that the filament bleed present in the parts printed on the Ender 5 system affected the electrical isolation of the Faraday plate. Because the ToolChanger system produced higher quality and faster prints, test personnel decided to continue with only that system for the single-process drift tube.

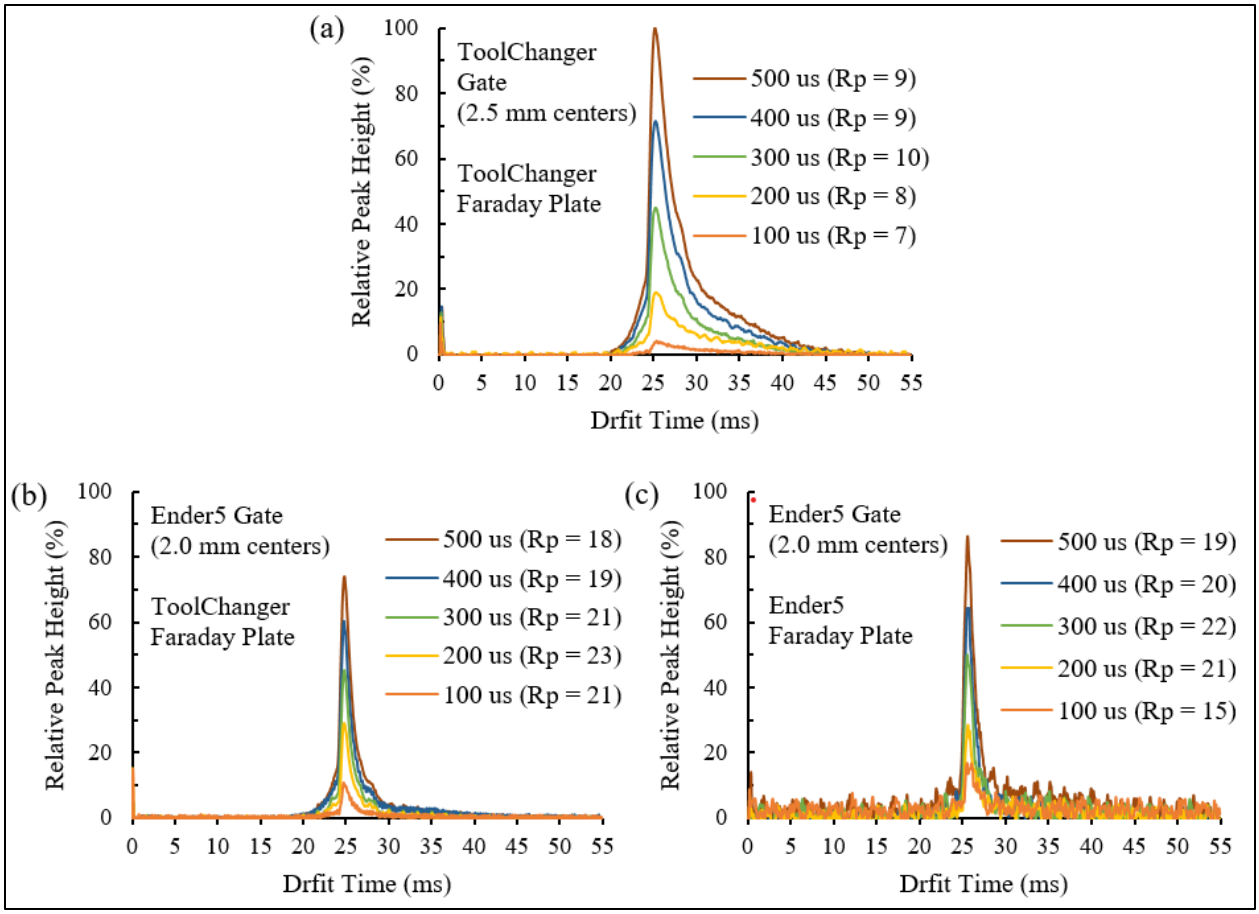

Figure 7. Drift time spectra of the $H(NH_3)^+ \bullet (H_2O)_n$ reactant ion peak at varying GPWs when using (a) the gate and Faraday plate printed on the ToolChanger system, (b) the gate printed on the Ender 5 system and the Faraday plate printed on the ToolChanger system, and (c) the gate and Faraday plate printed on the Ender 5 system.

3.2 Single-Process Unibody Drift Tube

The single-process unibody drift tube shown in Figure 8a was printed by the ToolChanger system in 52 h 7 min. The photograph was taken before dissolution, so PVA can be seen behind the wires of the corona ionization counter electrode. After dissolution and cleaning, the drift tube was connected to the data acquisition and electrical systems to collect spectra. D*t*BP was introduced, and spectra were collected at 280 V/cm with a 200 µs GPW. The reactant and product ion peaks appeared at 19.4 and 30.3 ms, respectively, with R_p values of 17 and 27, respectively (Figure 8a; blue). D*t*BP was readily eliminated from the drift tube by the drift gas, and the time it took to return the spectrum to background was comparable to that for instruments constructed by traditional means. An ideal drift voltage was calculated for a 100 µs GPW based on the work of Kirk and coworkers,[19] and the reactant and product ion peaks shifted to 13.4 ms and 20.9 ms, respectively, with R_p values of 26 and 36, respectively, at 424 V/cm (Figure 8b; red). Commercial ambient pressure IMS instruments with short drift tubes have historically been able to achieve an R_p between 30 and 40, whereas research-grade instruments have achieved upward of 150 with the aid of pre or post separation.[20, 21] The R_p of the single-process unibody

drift tube is currently comparable to these small commercial systems and the modular drift tube 3D printed by Drees and coworkers.[10] However, it is expected that the R_p can be increased by improving the gate design with narrower wires and optimized wire spacing while maintaining structural integrity during dissolution, cleaning, and operation.

Twenty-two D*t*BP spectra, each consisting of 100 iterations of 20 averages, at various GPWs between 100 and 300 µs, and at 280 V/cm, were collected across two days. An accurate K_0 value of 1.477 for D*t*BPH$^+$ was used to back calculate the length of the drift tube.[22] The average back-calculated length was 14.10 ± 0.02 cm, equating to the designed length plus or minus one printed layer height. This further indicates that 3D printing is a highly precise and accurate method for drift tube construction, as previously shown.[9]

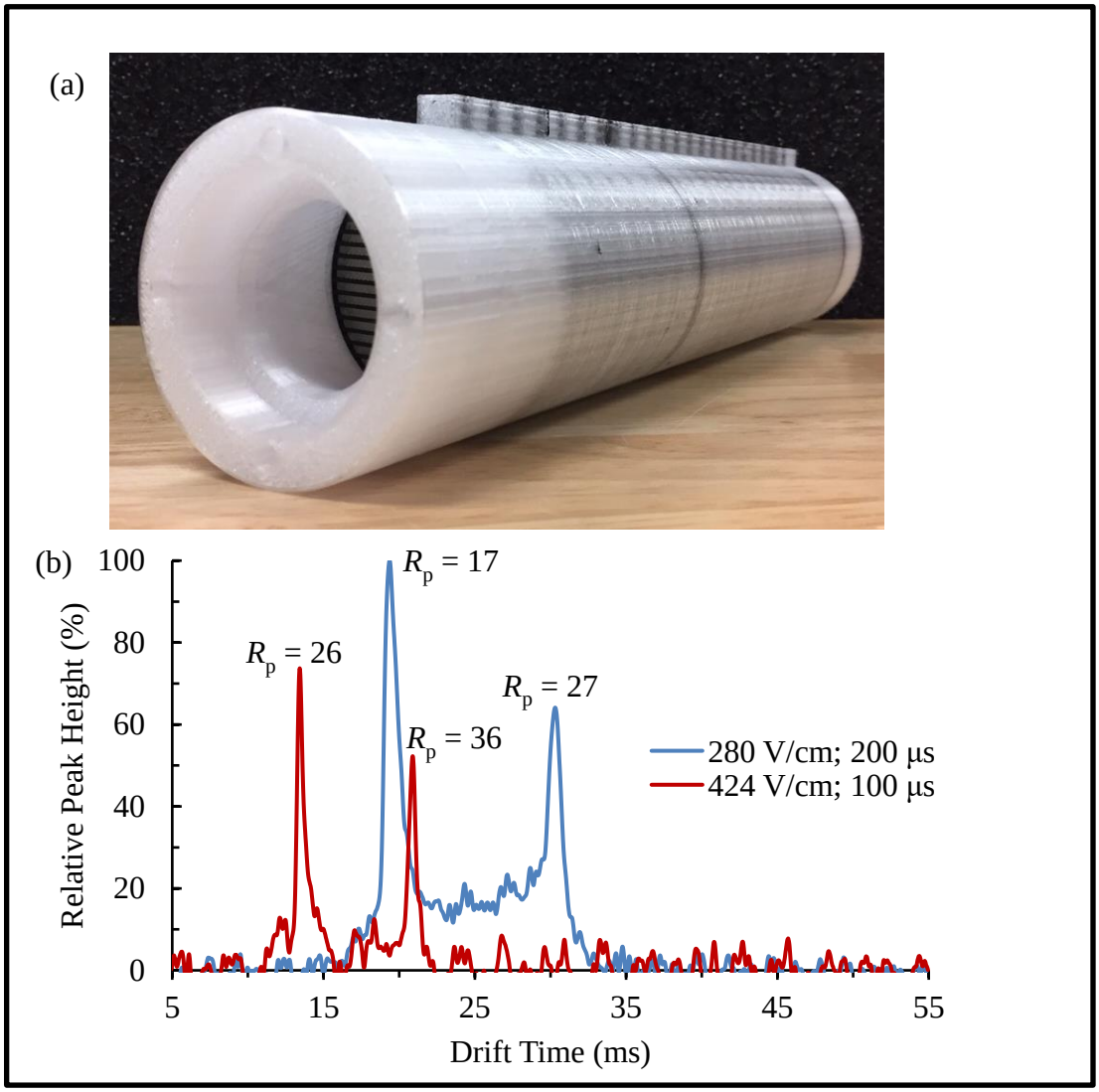

Figure 8. (a) Completed single-process unibody drift tube before dissolution of PVA and (b) D*t*BP spectra collected at 280 V/cm with a 200 µs GPW (blue) and at 424 V/cm with a 100 µs GPW (red).

4. CONCLUSIONS

In this report we have demonstrated, for the first time, the ability to 3D print an IMS drift tube containing freestanding gate wires in a single process. This was done by using a 3D printing system capable of utilizing at least three filaments, with one of those filaments being a soluble support. The ToolChanger system produced faster and higher quality prints with less waste than the combined Palette 2 multi-filament splicer and Ender 5 3D printer. When an ESD filament is 3D printed, the extrusion temperature and speed affects the conductivity of the filament, and the same settings may produce different conductivities on different 3D printers. It is, therefore, important to test these parameters with each new filament and printer. The drift tube presented here has an advantage over modular 3D-printed designs in that it is a single process and does not require any assembly of subcomponents. The drift length from ion gate to Faraday plate can be determined with high certainty based on the design of the drift tube, and any error that may have been introduced through the assembly of modular components is eliminated. The performance of the drift tube described in this report is comparable to that of some commercial systems, and it is expected that performance can be improved through rapid prototyping. Design improvements and spectra quality with various samples will be investigated in future studies.

LITERATURE CITED

1. Ligon, S.C.; Liska, R.; Stampfl, J.; Gurr, M.; Mülhaupt, R. Polymers for 3D Printing and Customized Additive Manufacturing. *Chem. Rev.* **2017,** *117*, 10212–10290.

2. Guillén-Alonso, H.; Rosas-Román, I.; Winkler, R. The Emerging Role of 3D Printing in Ion Mobility Spectrometry and Mass Spectrometry. *Anal. Methods* **2021,** *13*, 852–861.

3. Eiceman, G.A.; Karpas, Z.; Hill, H.H., Jr. *Ion Mobility Spectrometry*. 3rd ed.; CRC Press: Boca Raton, FL, 2014.

4. Weston, D.J.; Bateman, R.; Wilson, I.D.; Wood, T.R.; Creaser, C.S. Direct Analysis of Pharmaceutical Drug Formulations Using Ion Mobility Spectrometry/Quadrupole-Time-of-Flight Mass Spectrometry Combined with Desorption Electrospray Ionization. *Anal. Chem.* **2005,** *77*, 7572–7580.

5. Ewing, R.G.; Atkinson, D.A.; Eiceman, G.A.; Ewing, G.J. A Critical Review of Ion Mobility Spectrometry for the Detection of Explosives and Explosive Related Compounds. *Talanta* **2001,** *54* (3), 515–529.

6. Eiceman, G.A.; Stone, J.A. Ion Mobility Spectrometers in National Defense. *Anal. Chem.* **2004,** *76* (21), 390A–397A.

7. Mäkinen, M.A.; Anttalainen, O.A.; Sillanpää, M.E.T. Ion Mobility Spectrometry and Its Applications in Detection of Chemical Warfare Agents. *Anal. Chem.* **2010,** *82* (23), 9594–9600.

8. Zhang, X.; Quinn, K.; Cruickshank-Quinn, C.; Reisdorph, R.; Reisdorph, N. The Application of Ion Mobility Mass Spectrometry to Metabolomics. *Curr. Opin. Chem. Biol.* **2018,** *42*, 60–66.

9. Hauck, B.C.; Ruprecht, B.R.; Riley, P.C.; Strauch, L.D.,III. Reproducible 3D-Printed Unibody Drift Tubes for Ion Mobility Spectrometry. *Sens. Actuators B* **2020,** *323*, 128671.

10. Drees, C.; Höving, S.; Vautz, W.; Franzke, J.; Brandt, S. 3D-Printing of a Complete Modular Ion Mobility Spectrometer. *Mater. Today.* **2021,** *44*, 58–68.

11. Poor Bridging. https://www.simplify3d.com/support/print-quality-troubleshooting/poor-bridging/ (accessed April 2021).

12. Poor Bridging. https://help.prusa3d.com/en/article/poor-bridging_1802 (accessed April 2021).

13. Bridging. https://support.ultimaker.com/hc/en-us/articles/360012112659-Bridging (accessed April 2021).

14. Hollerbach, A. Baird, Z.; Cooks, R.G. Ion Separation in Air Using a Three-Dimensional Printed Ion Mobility Spectrometer. *Anal. Chem.* **2017,** *89* (9), 5058–5065.

15. Hollerbach, A.; Fedick, P.W.; Cooks, R.G. Ion Mobility-Mass Spectrometry Using a Dual-Gated 3D Printed Ion Mobility Spectrometer. *Anal. Chem.* **2018,** *90* (22), 13265–13272.

16. Chen, C.; Tabrizhi, M.; Li, H. Ion Gating in Ion Mobility Spectrometry: Principles and Advances. *TrAC, Trends Anal. Chem.* **2020,** *133*, 116100.

17. Brunner, T.; Mueller, A.R.; O'Sullivan, K.; Simon, M.C.; Kossick, M.; Ettenauer, S.; Gallant, A.T.; Mané, E.; Bishop, D.; Good, M.; Gratta, G.; Dilling, J. A Large Bradbury Nielson Ion Gate with Flexible Wire Spacing Based on Photo-Etched Stainless Steel Grids and its Characterization Applying Symmetric and Asymmetric Potentials. *Int. J. Mass Spectrom.* **2012,** *309*, 97–103.

18. Siems, W.F.; Wu, C.; Tarver, E.E.; Hill, H.H., Jr.; Larsen, P.R.; McMinn, D.G. Measuring the Resolving Power of Ion Mobility Spectrometers. *Anal. Chem.* **1994,** *66*, 4195–4201.

19. Kirk, A.T.; Bakes, K.; Zimmermann, S. A Universal Relationship Between Optimum Drift Voltage and Resolving Power. *Int. J. Ion Mobility Spectrom.* **2017,** *20*, 105–109.

20. Kanu, A. B.; Gribb, M.M.; Hill, H.H., Jr. Predicting Optimal Resolving Power for Ambient Pressure Ion Mobility Spectrometry. *Anal. Chem.* **2008,** *80*, 6610–6619.

21. Tolmachev, A.V.; Clowers, B.H.; Belov, M.E.; Smith, R.D. Coulombic Effects in Ion Mobility Spectrometry. *Anal. Chem.* **2009,** *81*, 4778–4787.

22. Hauck, B.C.; Harden, C.S.; McHugh, V.M. Accurate Evaluation of Potential Calibration Standards for Ion Mobility Spectrometry. *Anal. Chem.* **2020,** *92* (8), 6158–6165.

ACRONYMS AND ABBREVIATIONS

3D	three-dimensional
BN	Bradbury–Nielson
BNC	Bayonet Neill-Concelman
CAD	computer-aided design
DI	deionized
D*t*BP	2,6-di-*tert*-butylpyridine
D*t*BPH$^+$	protonated ion of D*t*BP
ESD	electrostatic dissipative
FDM	fused deposition modeling
.gcode	G-code
GPW	gate pulse width
$H(NH_3)^+•(H_2O)_n$	ammonium reactant ion with *n* water clusters
i.d.	inside diameter
IMS	ion mobility spectrometry
K_0	reduced ion mobility value
L	drift length
.maf	mutation annotation format
o.d.	outside diameter
P	drift gas pressure
PETG	polyethylene terephthalate glycol-modified
PVA	polyvinyl alcohol
R_p	resolving power
.stl	stereolithography
SR	soluble release
T	drift gas temperature
t_d	ion drift time
TP	Tyndall–Powell
V	voltage gradient

DISTRIBUTION LIST

The following individuals and organizations were provided with one Adobe portable document format (pdf) electronic version of this report:

U.S. Combat Capabilities Development Command Chemical Biological Center (DEVCOM CBC)
FCDD-CBR-ID
ATTN: Hauck, B.
Riley, P.
Wade, M.

FCDD-CBE-E
ATTN: Ruprecht, B.
Moore, R.

DEVCOM CBC
Technical Library
FCDD-CBR-L
ATTN: Foppiano, S.
Stein, J.

Defense Technical Information Center
ATTN: DTIC OA

U.S. ARMY COMBAT CAPABILITIES DEVELOPMENT COMMAND
CHEMICAL BIOLOGICAL CENTER